uc3m | Universidad Carlos III de Madrid

e-Archivo

This is a postprint version of the following published document:

Merino, M.; Ahedo, E. Effect of the plasma-induced magnetic field on a magnetic nozzle, In: *Plasma sources science and technology, 25, 045012, June 2016, 9 pp.*

DOI: https://doi.org/10.1088/0963-0252/25/4/045012

© 2016 IOP Publishing Ltd.

Effect of the Plasma-induced Magnetic Field on a Magnetic Nozzle

Mario Merino, Eduardo Ahedo

Equipo de Propulsión Espacial y Plasmas (EP2), Universidad Carlos III de Madrid, 28911 Leganés, Spain

E-mail: mario.merino@uc3m.es

Abstract. A two-fluid, two-dimensional model of the plasma expansion in a divergent magnetic nozzle is used to investigate the effect of the plasma-induced magnetic field on the acceleration and divergence of the plasma jet self-consistently. The induced field is diamagnetic and opposes the applied one, increasing the divergence of the magnetic nozzle and weakening its strength. This has a direct impact on the propulsive performance of the device, the demagnetization and detachment of the plasma, and can lead to the appearance of zero-field points and separatrix surfaces downstream. In contrast, the azimuthal induced field, albeit non-zero, is small in all cases of practical interest.

1. Introduction

A Magnetic Nozzle (MN) is an axisymmetric, longitudinal magnetic field with a convergent-divergent (or merely divergent) geometry that can guide, expand and accelerate a sonic plasma[1, 2, 3, 4, 5, 6]. MNs are promising for space plasma propulsion thanks to their ability to accelerate and control in-flight a high velocity plasma jet contactlessly. As a consequence, several next-generation plasma thrusters being actively developed employ a MN as their main acceleration stage[7, 8, 9, 10, 11, 12]. Once the plasma has been accelerated by the MN, it needs to detach itself from the influence of the closed magnetic lines to form a free plasma plume before these begin to turn around to close upon themselves[13, 14, 15]. This is not a problem for other applications of MNs such as advanced manufacturing and material plasma processing[16, 17] or plasma wind tunnels[1], where the goal is to direct the plasma jet against a material target in a controlled manner.

To obtain the desired "nozzle" effect and guide the plasma along the magnetic lines requires that at least the electrons be well magnetized in the near region of the MN (i.e., approximately until the MN turning point where the outermost magnetic lines start turning around). This is ensured in current devices, which use magnetic fields in the order of a few hundreds of Gauss. The applied magnetic field strength is nonetheless insufficient to magnetize the heavier ions in the cases of interest, except perhaps near the throat region. In this regime, electrons faithfully follow the magnetic tubes, and ions

expand and accelerate thanks to the ambipolar plasma electric field that ensues[6, 18]. Unmagnetized ions downstream are also a requirement for adequate plasma detachment in propulsive applications[15].

The electric currents that exist in the plasma induce a magnetic field, whose relative intensity with respect to the applied one scales with the β parameter of the plasma. As the plasma density is increased, so does its β parameter, and at some point the plasma-induced field becomes a major feature of the expansion, which can alter and deform the shape of the MN and modifies its the field strength locally. The natural question that arises then is on the magnitude of these effects and their possible consequences on the operation of the MN, and in particular, on the downstream detachment of the plasma jet. Works by Arefiev and Breizman[19] and Winglee et al.[20] reported that the plasma-induced magnetic field reinforces and strengthens the applied field, reducing the MN divergence. In these theories, the induced field stretches the MN downstream to infinity. This has been proposed as a means to circumvent the plasma detachment problem, by which the plasma would actually carry the (frozen) magnetic field lines within itself. As the plasma drags and develops the magnetic lines, the turning point of the magnetic nozzle (i.e., the point where the outermost magnetic line turns around) would be "ironed out" to infinity and disappear.

That picture of the expansion presumes de facto a *paramagnetic* character of the plasma-induced magnetic field. However, a paramagnetic induced field means the existence of an attractive magnetic force between the plasma and the magnetic field generator at the thruster[21], resulting in negative thrust (i.e. magnetic drag) rather than positive thrust production. Clearly, in a propulsive MN the plasma must be dominantly *diamagnetic* so that it is repelled away from the thruster and magnetic thrust is generated[6, 22].

In fact, a plasma with warm magnetized electrons develops naturally a diamagnetic drift current proportional to the electron pressure, which arises from the collective effect of the individual gyromotion of each electron. As shown in previous works[6, 14, 15], this electron current in the azimuthal direction is fundamental for the radial confinement of the plasma expansion and the generation of magnetic thrust; on the other hand, the only reported paramagnetic contribution was the small azimuthal ion current that develops downstream as ions detach from the field lines. While this effect increases with the applied magnetic field strength and with the kinetic energy of ions, the ion paramagnetic current is upper-bounded[15], and indeed negligible with respect to the diamagnetic electron current except for the highest magnetization levels or if ions that enter the MN already at hypersonic velocities (i.e., a 'cold plasma' expansion), cases of little practical interest in most applications.

The major goal of this work is to prove from the framework of a consistent plasma expansion model that, instead of reinforcing and stretching the MN to infinity, the induced magnetic field (*i*) opposes the externally-applied field (*ii*) opens the magnetic tubes of the MN, *increasing* its divergence, and (*iii*) *weakens* the magnetic strength of the MN, promoting the earlier demagnetization (and detachment) of the plasma.

This behavior is consistent with the diamagnetic character of the plasma discussed above. The article also characterizes the strong 2D nature of induced field effects, and comments on the capability of the plasma to reverse the direction of the magnetic field downstream and create regions where the applied field has been completely expelled. Both the longitudinal and the azimuthal induced magnetic fields are addressed.

The rest of this paper is structured as follows. Section 2 presents a 2D plasma/MN model with induced magnetic field. Section 3 discusses the longitudinal induced magnetic field in a simplified paraxial geometry to identify its key effects on the MN. Section 4 integrates the full 2D model using an iterative scheme for the solution of the self-consistent longitudinal and azimuthal induced field and conducts the parametric investigation of the expansion. Lastly, Section 5 highlights the main conclusions of this work.

2. Plasma expansion model

The two-fluid plasma/MN model introduced in Ref. [6] is extended here to include the plasma-induced magnetic field. The model describes the axisymmetric, collisionless, quasineutral expansion of a supersonic plasma composed of hot, fully-magnetized, isotropic, Maxwellian electrons and cold, single-charged ions in a divergent magnetic field. Extensions of the model to include non-Maxwellian electrons[23] and warm ions[24] can be found elsewhere. Those effects do not change qualitatively the conclusions herein, and therefore are not treated below.

For the sake of illustration, the applied field of the MN is that of a single current loop of radius R_L located in the plane $z = 0$. The plasma flows inside this magnetic field toward $z > 0$. We will denote the applied, plasma-induced, and total magnetic field as $\boldsymbol{B}_a$, $\boldsymbol{B}_p$, and $\boldsymbol{B} = \boldsymbol{B}_a + \boldsymbol{B}_p$ respectively. A subindex '0' indicates values at the origin ($z = r = 0$): e.g. $B_{a0} = B_{az}(0, 0)$. We choose $B_{a0} > 0$ without loss of generality. As in Ref. [6], a tilde will be used to indicate the longitudinal component of a vector field: e.g. $\tilde{\boldsymbol{B}} = B_z\mathbf{1}_z + B_r\mathbf{1}_r = \boldsymbol{B} - B_\theta\mathbf{1}_\theta$, and the right-handed magnetic reference frame is introduced: $\{\mathbf{1}_\parallel, \mathbf{1}_\perp, \mathbf{1}_\theta\}$, with $\mathbf{1}_\parallel = \tilde{\boldsymbol{B}}/\tilde{B}$ and $\mathbf{1}_\perp = \mathbf{1}_\theta \times \mathbf{1}_\parallel$. Since the magnetic field is solenoidal, there exists a streamfunction ψ for its longitudinal components: e.g. $\partial\psi/\partial r = rB_z$ and $\partial\psi/\partial z = -rB_r$. In the same manner we define ψ_a for the applied field and ψ_p for the induced one, so that $\psi = \psi_a + \psi_p$. By convention, we shall take $\psi_a = \psi_p = \psi = 0$ at the axis.

Electrons are modeled as an isotropic Maxwellian species with an effective polytropic cooling law, $p_e \propto n^\gamma$ (where $p_e = nT_e$ is the electron pressure, $\gamma \geq 1$ is the polytropic cooling exponent, n the (quasineutral) plasma density, and T_e is the electron temperature). The value of γ that best approximates the behavior of the electron species seems to depend on the experimental setup, and ranges from near-isothermal values[4, 25] (< 1.1 to 1.3) to near-adiabatic values[26] (5/3). Recent kinetic models[27, 28] suggest that a variable γ that is close to unity in the near region and increases downstream can accurately describe electron cooling. Under the assumption

that $m_e u_e^2 \ll T_e$ (i.e., negligible electron inertia with respect to thermal motion) and $\ell_e \ll L$ (i.e., electron Larmor radius ℓ_e small compared to the macroscopic scale length, L), electron streamtubes coincide with magnetic streamtubesRef. [6]. Observe, however, that electrons now follow the *total* magnetic field $\boldsymbol{B}$ instead of merely the applied one. Keeping only the non-zero components of the magnetic force on electrons, these equations read:

$$n\tilde{u}_e/B = G_e(\psi); \quad \tilde{\boldsymbol{u}}_e = u_{\parallel e}\mathbf{1}_\parallel \quad \text{(i.e.: } u_{\perp e} = 0\text{)}, \tag{1}$$

$$0 = -\gamma T_e \nabla \ln \frac{n}{n_0} + e\nabla\phi - e\left(u_{\theta e}\tilde{B} - u_{\parallel e}B_{\theta p}\right)\mathbf{1}_\perp, \tag{2}$$

where $G_e(\psi)$ is the electron flux-to-magnetic strength ratio on each streamtube, $\boldsymbol{u}_e$ the electron velocity, e the electron charge, and ϕ the ambipolar electric potential. The projection of the last equation along $\mathbf{1}_\parallel$ can still be integrated into:

$$H_e(\psi) = \begin{cases} \gamma T_e/(\gamma - 1) - e\phi & \text{if } \gamma > 1, \\ T_{e0}\ln(n/n_0) - e\phi & \text{if } \gamma = 1, \end{cases} \tag{3}$$

with $H_e(\psi)$ the Bernoulli function on each streamtube. Finally, the projection of Eq. (2) along $\mathbf{1}_\perp$ reads:

$$eu_{\theta e}\tilde{B} - eu_{\parallel e}B_{\theta p} = -\frac{\partial H_e}{\partial \mathbf{1}_\perp} \equiv -r\tilde{B}\frac{\mathrm{d}H_e}{\mathrm{d}\psi}. \tag{4}$$

As a side note, observe that the isorotation condition of the electron flow[29, 30] (i.e., $u_{\theta e}/r = \text{const}$ along magnetic tubes) is only satisfied for $B_{\theta p}/\tilde{B} \to 0$, and that a positive $B_{\theta p}/\tilde{B}$ tends to increase $u_{\theta e}/r$.

The steady-state motion of ions is given by their continuity and momentum equations,

$$\nabla \cdot (n\boldsymbol{u}_i) = 0, \tag{5}$$

$$m_i(\boldsymbol{u}_i \cdot \nabla)\boldsymbol{u}_i = -e\nabla\phi + e\boldsymbol{u}_i \times \boldsymbol{B} \tag{6}$$

where m_i and $\boldsymbol{u}_i$ are respectively the ion mass and the ion velocity. By projecting Eq. (6) along $\boldsymbol{u}_i$ and $\mathbf{1}_\theta$ one obtains

$$m_i\frac{u_i^2}{2} + e\phi = H_i(\psi_i), \tag{7}$$

$$rm_i u_{\theta i} + e\psi = D_i(\psi_i), \tag{8}$$

where ψ_i is the ion streamfunction that labels each ion streamtube and $H_i(\psi_i)$, $D_i(\psi_i)$ are the ion mechanical energy and the canonical angular momentum on each ion streamtube. The radius of the plasma, i.e. that of the plasma-vacuum interface, is denoted as $R_V(z)$. At the throat section ($z = 0$) the plasma is sonic and has a radius $R_0 < R_L$. This is expressed by the ion Mach number at the origin, $M_0 = \tilde{u}_{i0}/c_{s0} = 1$, with $c_{s0} = \sqrt{\gamma T_{e0}/m_i}$ the ion sonic velocity.

Finally, Ampère's law $\nabla \times \boldsymbol{B}_p = \mu_0 \boldsymbol{j}$ relates the induced magnetic field to the electric currents in the plasma, $\boldsymbol{j} = en\left(\boldsymbol{u}_i - \boldsymbol{u}_e\right)$. Written in terms of ψ_p and $B_{\theta p}$, this equation becomes:

$$\frac{1}{r}\frac{\partial^2 \psi_p}{\partial z^2} + \frac{\partial}{\partial r}\left(\frac{1}{r}\frac{\partial \psi_p}{\partial r}\right) = -\mu_0 j_\theta, \tag{9}$$

$$\frac{1}{r}\frac{\partial}{\partial r}\left(rB_{\theta p}\right) = \mu_0 j_z; \quad \frac{\partial B_{\theta p}}{\partial z} = -\mu_0 j_r, \tag{10}$$

with $B_{\theta p}(z,0) = 0$. Equations (9) and (10) show that $\tilde{\boldsymbol{B}}_p$ is caused only by the azimuthal plasma current j_θ, while $B_{\theta p}$ can be calculated from j_z alone.

The plasma momentum equation (i.e., the sum of Eqs. (2) and (6)),

$$m_i\left(\boldsymbol{u}_i \cdot \nabla\right)\boldsymbol{u}_i = -\gamma T_e \nabla \ln\frac{n}{n_0} + \frac{\boldsymbol{j}}{n} \times \boldsymbol{B}, \tag{11}$$

shows that radial equilibrium at the throat requires $j_\theta \sim nT_e/(R_0 B)$. Introducing this into Ampère's equation (9) it can be seen that

$$\frac{\tilde{B}_p}{B_a} \sim \mu_0 \frac{nT_e}{B_a^2} = \beta_a, \tag{12}$$

where β_a is the well-known thermal beta parameter based on the applied field, which is a measurement of the capability of the plasma to generate an induced magnetic field of sufficient strength to disturb the MN. Note that a factor 2 is sometimes included in this definition, but it is purposely omitted here.

Normalization of the model shows that the plasma expansion depends on:(*i*) the ratio R_0/R_L, which controls the divergence rate of the outermost magnetic line where plasma exists and the position of the turning point of the applied field; (*ii*) the radial plasma profile at the throat; (*iii*) the 'effective electron cooling rate,' measured by γ; (*iv*) the ion dimensionless gyrofrequency at the origin, $\hat{\Omega}_{i0} = eB_{a0}R_0/\sqrt{m_i T_{e0}}$, which controls the applied field magnetic strength; and (*v*) the *plasma beta parameter at the origin*, defined as $\beta_{a0} = \mu_0 n_0 T_{e0}/B_{a0}^2$. The first four dependencies have already been discussed in previous works[6, 24]; the fifth parameter is the fundamental one in the present discussion.

3. Paraxial 1D plasma expansion

The order of magnitude estimation in Eq. (12) already reveals the main dependencies of the relative role induced magnetic field. Before carrying out the full 2D integration of the model, we can gain some physical insight on the problem by solving the analytical, paraxial expansion limit, that is, when the characteristic axial gradient length is $L_z \gg R_0$. This requires a slender and slowly-varying applied magnetic field, so that $u_{ri} \ll u_{zi}$ and $\mathbf{1}_\perp \simeq \mathbf{1}_r$. In practice, this is only true for a limited length and for $R_L/R_0 \gg 1$.

For simplicity, we will assume that the radial plasma profile is uniform and treated the expansion as 1D in first approximation. We shall further assume that ions do not have an initial rotation, so that, according to Eq. (8), $u_{\theta i} \simeq 0$ everywhere in the paraxial limit. In this case, $j_\theta = 0$ except at the plasma edge, where the electron diamagnetic drift current concentrates in a thin sheet of thickness $\mathcal{O}(\ell_e) \ll R_0$ as shown in Ref. [6].

The ion equations of the model become simple algebraic relations:

$$nu_{zi}/B = G_i, \tag{13}$$

$$\frac{1}{2}m_i u_{zi}^2 + e\phi = H_i, \tag{14}$$

where G_i, the ion-to-magnetic flux, and H_i, the ion Bernoulli function, are two upstream constants. Combining the last equation with Eq. (3) allows to eliminate ϕ. Note that H_e is now a single constant for all streamtubes. Neglecting radial ion inertia, the radial plasma momentum equation (Eq. (6) plus Eq. (2), projected along $\mathbf{1}_r$) can be integrated into

$$nT_e = \int_{layer} j_\theta(r)B(r)dr, \tag{15}$$

where the integration takes place across the current-sheet layer at the plasma border. Since the paraxial limit of Ampère's equation states that

$$\frac{dB}{dr} = \mu_0 j_\theta, \tag{16}$$

we can write this expression as

$$2\mu_0 nT_e = B_{ext}^2 - B_{int}^2, \tag{17}$$

where B_{ext} and B_{int} are the strength of the magnetic field immediately outside and inside of the plasma tube.

This last equation shows that a discontinuity in the magnetic field exist across the current sheet in the macroscopic scale, which depends only on the local electron pressure at each section. This result can be interpreted as follows: the diamagnetic current induces a field B_p that opposes the applied one, reducing the magnetic strength inside the plasma, and in doing so, expelling a fraction of the magnetic flux out of it.

To close the paraxial model analytically, we need to consider the following additional approximation: the azimuthal current sheet in the plasma forms a very long tube whose radius and intensity varies only slowly, according to $L_z \gg R_0$. As such, to first order, the magnetic field it induces is restricted to the inside of the tube, just like an infinite solenoid. Under this assumption we can identify $B_{ext} = B_a$, the applied field, and $B_{int} = B = B_a + B_p$, the total magnetic field in the plasma. Then,

$$B^2/B_a^2 = 1 - 2\beta_a, \tag{18}$$

where again $\beta_a = \mu_0 nT_e/B_a^2$ is the *local* beta parameter based on B_a. A higher β_a clearly means a stronger induced field and therefore a lower total field, i.e. a weaker MN. Since

β_a depends on the local electron pressure, the determination of B is coupled with the integration of the plasma expansion.

Naturally, two questions arise: first, whether β_a increases downstream so that B_p gains importance with respect to B_a, and second, whether the presence of induced field effects means a faster-diverging MN all the way to infinity. Rearranging Eq. (17),

$$\frac{1}{\beta_a} = 2 + \frac{B^2}{\mu_0 n T_e} = 2 + \frac{B^2}{\mu_0 n_0 T_{e0}} \frac{n_0^\gamma}{n^\gamma}. \tag{19}$$

Hence, β_a increases if n^γ decreases slower than B^2. The ordering of n can be easily obtained from Eq. (13), noting that far downstream,

$$u_{zi} \to \sqrt{\frac{\gamma T_{e0}}{m_i} \frac{\gamma+1}{\gamma-1}}, \tag{20}$$

i.e., a finite value when $\gamma \neq 1$. Hence, $n \propto B$ in the far expansion region. This means that β_a increases downstream for $\gamma < 2$, and therefore so does the induced magnetic field with respect to the applied one. [Note that in the isothermal case, $u_{zi} \sim \sqrt{-2(T_{e0}/m_i)\ln(n/n_0)}$ downstream instead, but the conclusion is still the same]. Clearly, a higher value of γ, i.e., a faster electron cooling, diminishes the relevance of the induced field in the far expansion region.

To answer the second question, observe that the evolution of $R_V(z)$ is given by $R_V(z)/R_0 = \sqrt{B_0/B(z)}$. Note, however, that in this model the value of B_0 depends on β_{a0} (i.e., the induced field can lower the value of B_0); moreover, the position of the MN throat itself may not coincide with the throat of the applied field. Nonetheless, comparing R_V against the case $\beta_{a0} = 0$, for which $R_V(z) = R_V(z)|_{\beta_{a0}=0}$, it can be seen that

$$\frac{R_V^4|_{\beta_{a0}=0}}{R_V^4} \propto \frac{B^2}{B_a^2}. \tag{21}$$

Hence, using Eq. (18) and since β_a increases downstream for $\gamma < 2$, so does $R_V/\ R_V|_{\beta_{a0}=0}$, and therefore the presence of an induced magnetic field results in a more divergent MN as $z \to \infty$.

The resulting model is completely algebraic and depends only on the parameters β_{a0} and γ. Figure 1 shows the shape of the resulting 1D MN shape and the value of $B(z)$ for several values of these parameters, illustrating the weakening and opening of the MN downstream. As it can be observed, the effect of the induced field is maximal for an isothermal plasma, and increases with β_{a0}. A small displacement of the actual magnetic throat toward the downstream side takes place, which only becomes significant at larger values of β_{a0}. All these phenomena can be regarded as the consequence of the diamagnetic nature of the plasma, which pushes against the applied magnetic field lines in the radial direction until a balance between the thermal pressure, nT_e, and the magnetic pressure, $B^2/(2\mu_0)$, is established.

While it provides valid trends in the low- and mild-β_a range, the quasi-1D model of this section suffers several limitations. First and foremost, the paraxial assumption

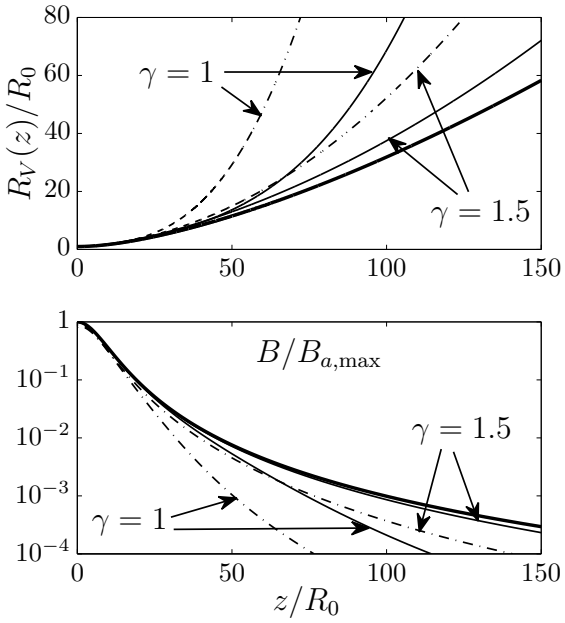

Figure 1. Plasma tube radius $R_V(z)$ and total magnetic field inside the plasma B in the paraxial limit, for $\beta_{a0} = 0$ (thick lines), $\beta_{a0} = 0.01$ (thin solid lines) and $\beta_{a0} = 0.1$ (dash-dot lines), and for $\gamma = 1$ and 1.5. For the purposes of presenting the results on a physical axial coordinate only, the axial magnetic field of a single current loop with $R_L = 10R_0$ has been used.

is not a valid one in actual devices, where 2D effects can play an important role in the expansion and there is a prominent turning-point for all magnetic lines except the central one; obviously, the turning point is missed in this approximation. Second, by keeping only the radial derivative in Eq. (16) this assumption has disregarded the elliptic character of Eq. (9) and considered only the local plasma currents for the determination of B_p; instead, in a 2D case the plasma currents at one point affect the magnetic field everywhere. Third, by dropping the radial ion inertia from Eq. (6) and assuming fully-magnetized ions, we have neglected the only paramagnetic current contribution in our model, i.e., the $j_{\theta i}$ that develops downstream. Nonetheless, as shown elsewhere[15, 24], the magnitude of this paramagnetic current is upper-bounded, and moreover, in the parametric range of practical interest for propulsive applications, it is always small ($j_{\theta i} \ll j_{\theta e}$). As a side comment, it is worth pointing out that radial ion inertia is central in the radial balance between the magnetic and electric forces on ions which determines the divergence of the ion streamlines and plasma detachment downstream. Without it, the computed ambipolar electric field is inconsistent in 2D models and the problem of detachment cannot be correctly analyzed[31]. Fourth, since the paraxial model does not allow the calculation of ion separation from the magnetic lines, it cannot recover the local longitudinal electric currents that develop in the plasma, and therefore cannot calculate $B_{\theta p}$. All these drawbacks, and the desire to study the radial variation of B_p, serve as the motivation to approach the analysis of the induced magnetic field effects

with the full 2D treatment of the next section.

4. 2D integration and discussion

The DIMAGNO code[6], which uses the method of characteristics (MoC) to integrate the hyperbolic ion equations of the supersonic expansion, has been extended to solve for the plasma-induced magnetic field $\boldsymbol{B}_p$ and include the additional magnetic force terms in the ion and electron equation due to B_θ. Due to the elliptic character of Eq. (9), simultaneous integration of both plasma and induced field would require abandoning the advantageous MoC approach. Instead, a convenient iterative procedure is used: an initial $\boldsymbol{B}_p$ is assumed (e.g. $\boldsymbol{B}_p = 0$), and a first plasma solution is obtained. The resulting plasma currents $\boldsymbol{j}$ are then used to refine the first estimate of $\boldsymbol{B}_p$: the plasma domain is discretized into small cells, and the current of each cell is represented by an infinitesimal current loop. The analytic solution of Ampère's equation (Eq. (9)) for such a loop is then used to compute each cell contribution to $\boldsymbol{B}_p$ in an efficient manner. Feeding the induced magnetic field back into the MN model, the process is repeated until convergence in $\boldsymbol{B}_p$ and the plasma variables is achieved[32].

The numeric integration of the MN plasma flow and $\boldsymbol{B}_p$ is carried out in the region between the throat and a downstream section $z = z_F$. Clearly, the plasma currents that exist upstream and downstream of this region can still affect what occurs within it, although, the magnetic influence of these currents decays quadratically with distance. To compensate for the influence of downstream currents, the simulation results presented in this section refer only to roughly half of the integrated region, i.e. for $z < z_F/2$, and it has been checked that the plasma expansion and the magnetic field in the presented region are nearly insensitive to the extension of the integration region. On the other hand, the influence of the plasma currents upstream of the MN throat, which depend on the type of plasma source used, is neglected, on the basis that the applied field is strongest in this region and therefore the induced field effects there are small in the β_{a0} range under study.

To simplify the discussion in the rest of this section, only the isothermal case is considered ($\gamma = 1$). The following plasma profile is assumed at the MN throat for $r < R_0$,

$$n(0,r) = n_0 \exp\left(-3r^2 \ln 10\right), \tag{22}$$

$$u_{zi}(0,r) = u_{ze}(0,r) = M_0\sqrt{T_{e0}/m_i}, \tag{23}$$

$$u_{ri}(0,r) = u_{re}(0,r) = u_{\theta i}(0,r) = 0, \tag{24}$$

$$\phi(0,r) = 0, \tag{25}$$

and it is injected into a MN with $R_L = 3.5R_0$ and $\hat{\Omega}_{i0} = 1$. To guarantee hyperbolicity in the whole plasma domain we enforce $M_0 = 1.01$. Equation (4) at the throat is used to determine the profile of $u_{\theta e}$,

$$u_{\theta e} = -\frac{6T_{e0}\ln 10}{e\tilde{B}}r \tag{26}$$

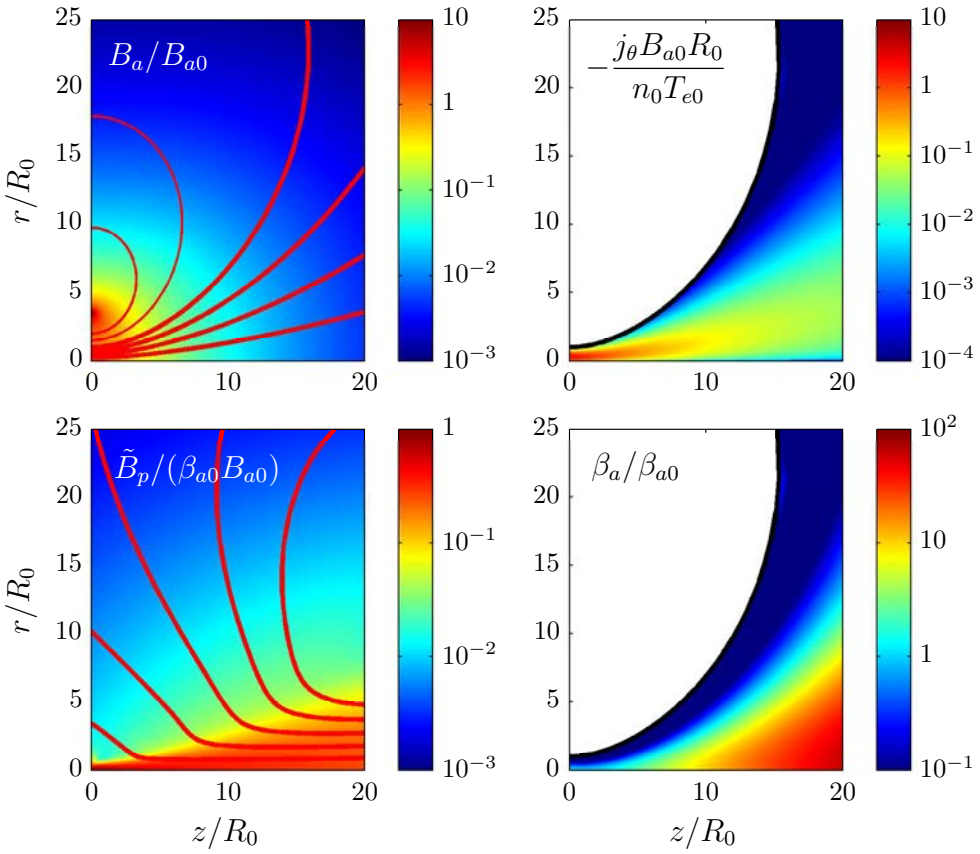

Figure 2. Applied field $\boldsymbol{B}_a$, induced field $\tilde{\boldsymbol{B}}_p$, azimuthal plasma current j_θ and local plasma beta β_a in the $\beta_{a0} = 0.01$ case ($\gamma = 1$, $R_L/R_0 = 3.5$, $\hat{\Omega}_{i0} = 1$). In the first two graphs, red lines show the direction of the magnetic field ($\boldsymbol{B}_a$ and $\tilde{\boldsymbol{B}}_p$ oppose each other at the axis). The normalization factors used in the figures remove the dominant dependencies of each plotted variable.

(observe that $B_{\theta p} = 0$ at the throat since we have chosen $j_z = 0$ at $z = 0$).

We begin the discussion with the longitudinal induced magnetic field, $\tilde{\boldsymbol{B}}_p$. The applied field $\boldsymbol{B}_a$, the self-consistent $\tilde{\boldsymbol{B}}_p$, the plasma current j_θ, and the local plasma beta for the case $\beta_{a0} = 0.01$ are depicted in Fig. 2.

The marked 2D character of the azimuthal plasma currents and the induced magnetic field stands out in these graphs. Both are larger in a region around the axis, while the periphery of the plasma is almost unaffected, especially downstream. Interestingly, while j_θ decreases gradually as n drops downstream as expected, $\tilde{B}_p$ maintains its strength, and the region around the axis where it is relatively large grows in size. It is easy to infer from these plots that the local value of $\tilde{B}_p/B_a$, i.e. the relative importance of induced field effects, increases fast downstream around the axis, in agreement with the 1D results, but only moderately so round the plasma edge. This behavior agrees well with the recovered 2D variation of the local β_a parameter in the

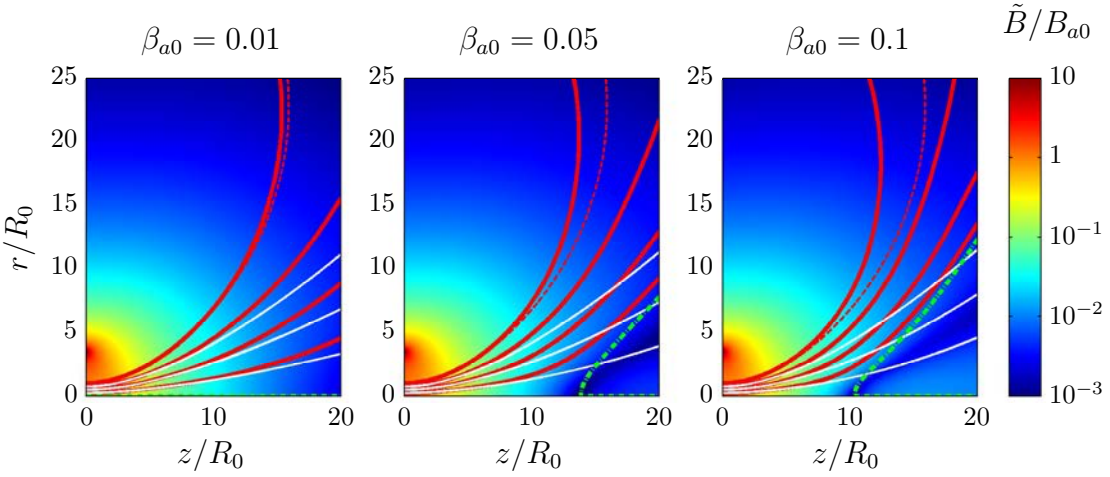

Figure 3. Total longitudinal magnetic field $\tilde{\boldsymbol{B}} = \boldsymbol{B}_a + \tilde{\boldsymbol{B}}_p$ in the MN for $\beta_{a0} = 0.01$, 0.05 and 0.1 ($\gamma = 1$, $\hat{\Omega}_{i0} = 1$, $R_L/R_0 = 3.5$). The plasma border and other magnetic streamtubes are indicated as thick red lines. Initially-coincident ion streamtubes are drawn as white, thin lines. For the purpose of comparison, the plasma border for the $\beta_{a0} = 0$ case is shown as a dashed red line. The existence of a magnetic separatrix is depicted as a dash-dot green line in the last two simulations.

last plot of Fig. 2, confirming its usefulness as an estimator of $\tilde{B}_p/B_a$, even if the actual value of $\tilde{B}_p$ results from the resolution of the elliptic Ampère's equation, Eq. (9).

The total longitudinal magnetic field is presented in Fig. 3 for $\beta_{a0} = 0.01$, 0.05, and 0.1. Two related phenomena take place and become more pronounced as β_{a0} increases, namely: (*i*) the increase of MN divergence caused by $\tilde{\boldsymbol{B}}_p$, and (*ii*) the reduction of the magnetic strength downstream. Once again, this is congruent with the (necessary) net diamagnetic character of the plasma in a propulsive MN and the generation of positive thrust and agrees with the results of the 1D model of Section 3.

Interestingly, if $\tilde{B}_p$ is large enough (i.e., for large enough values of β_{a0}), the total magnetic field can eventually cancel out downstream. This can be already observed for $\beta_{a0} = 0.05$ in Fig. 3, and is marked by the appearance of a point at the axis where $B = 0$, which has been also recovered experimentally[33]. In the region beyond this point, delimited by a separatrix surface (green dash-dot line), the direction of the magnetic field is reversed, and becomes induced-field dominated. This separatrix can therefore be regarded as an 'effective' end boundary of the MN. Since $\tilde{\boldsymbol{B}}_p$ does not substantially affect the strength of the peripheral plasma, the separatrix does not reach the plume edge within the simulated domain, but bends downstream.

Related to this, the weaker magnetic field boosts plasma demagnetization, especially at the core of the jet. Demagnetization of each species has a fundamentally different effect in the expansion: on the one hand, for the supersonic, mass-carrying ions it is a central mechanism for plasma detachment[15], as it allows the ions to separate inward from the magnetic tubes. This *self-demagnetization* of the central, densest

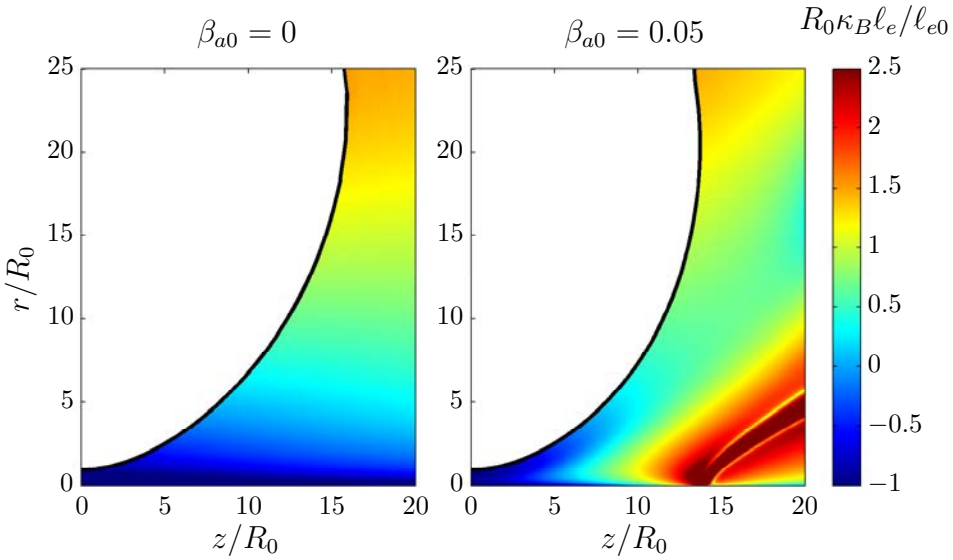

Figure 4. Normalized electron Larmor radius, $\ell_e = \sqrt{m_e T_e}/(eB)$, relative to the local magnetic length, $L_B = 1/\kappa_B$, for $\beta_{a0} = 0$ and 0.05. The graphs are normalized with the electron Larmor radius at the origin, ℓ_{e0} to make them more general. Typical values of ℓ_{e0}/R_0 in propulsive applications are within 10^{-2}–10^{-3} (Ref. [6]).

plasma therefore contributes to this detachment process and promotes the formation of a free-expanding plume, as ions are allowed to separate sooner from the magnetic lines.

On the other hand, premature demagnetization of the electrons can lead to increased plume divergence, as the beneficial magnetic force on electrons vanishes and electron confinement is tasked solely to the ambipolar electric field, which expands ions radially. If electron demagnetization occurs too soon (i.e., before ion acceleration is nearly complete and ions are highly hypersonic), this will result in a penalty on the propulsive performance of the MN. The magnetization degree of electrons is measured by the ratio of their local Larmor radius, ℓ_e, to the characteristic macroscopic magnitude of the problem. This can be taken to be the most critical one between R_0 and the local magnetic meridional curvature radius $L_B = 1/\kappa_B$, with κ_B the meridional magnetic field curvature. This quantity is plotted in Fig. 4 for $\beta_{a0} = 0$ and 0.05 for comparison. As it can be seen, ℓ/L_B can easily increase about 3 or more orders of magnitude downstream when $\boldsymbol{B}_p$ dominates (particularly if $B \simeq 0$ is reached). Fortunately, in the central part of the jet the electron pressure gradients are low, so this does not impose a heavy penalty on the performance of the MN. On the other hand, the sustained (higher) magnetic field at the peripheral plasma enables the MN to continue to confine the electron pressure in this region, where the gradients are largest, and can be regarded as a beneficial effect.

The effect of the enhanced MN divergence caused by $\tilde{\boldsymbol{B}}_p$ on the propulsive performance of the device can be observed in Fig. 5 with the plume efficiency function, $\eta_{plume}(z)$, defined in Ref. [6] as the ratio of axial to total ion kinetic power at a section

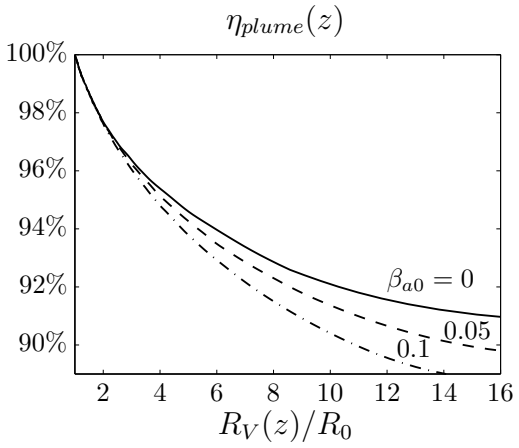

Figure 5. Evolution of the plume divergence efficiency $\eta_{plume}(z)$, for the simulations cases of Fig. 3. The solid line has $\beta_{a0} = 0.01$, and is visually indistinguishable from the $\beta_{a0} = 0$ case. The dashed line has $\beta_{a0} = 0.05$, and the dash-dot line has $\beta_{a0} = 0.1$.

$z = \text{const}$. Increasing β_{a0} decreases the efficiency, due to the larger radial plasma losses and plume divergence angle. Nonetheless, the effect is visibly small within the β_{a0} range of the present simulations; the reason for this lays in the already advanced state of ion detachment at the section where the changes in MN geometry become important. This is evidenced by the large separation of ion streamtubes with respect to magnetic streamtubes around $z/R_0 = 10$ to 15 in Fig. 3. Indeed, the divergence angle of the inner ion streamtubes is almost unaffected by the induced magnetic field, and the influence of the larger MN aperture is essentially limited to the low density peripheral plasma.

While the increased plume divergence decreases η_{plume}, the net effect over the thrust function $F(z)/F_0$, i.e., the impulse carried by the jet at a given section z, is smaller than a 1% for the analyzed range of β_{a0} (not shown). It should be kept in mind that the magnetic forces on the plasma due to the induced field itself, $j_\theta \tilde{B}_p$ and $\tilde{\jmath} B_{\theta p}$, are purely internal to the plasma, and therefore cannot contribute directly to thrust; these forces can only cause a redistribution of the plasma properties within the plasma domain.

We now turn our attention to the analysis of the azimuthal induced field, $B_{\theta p}$, generated by the longitudinal electric currents. For a plasma satisfying $j_z = 0$ at the throat, j_z develops downstream as the ion streamtubes separate, and therefore $B_{\theta p}$ is detachment-dependent, and a higher value of $\hat{\Omega}_{i0}$ reduces the magnitude of j_z everywhere[6]. While $j_z \to 0$ downstream due to the geometric expansion, $j_z/(enu_{zi})$ does not vanish in the region of validity of the model.

As ions separate inwards, $j_z > 0$ near the axis, while $j_z < 0$ near the jet boundary in order to satisfy global current ambipolarity. As long as this condition is satisfied (as in propulsive applications, where the net charge emitted by a thruster is zero in the steady-state), the integral $\int 2\pi r j_z dr$ vanishes at every $z = \text{const}$ section. Therefore, $B_{\theta p} = 0$ both at the axis and at the plasma edge: i.e., there is no induction of $B_{\theta p}$

outside of the plasma domain.

According to Eq. (10), $B_{\theta p} > 0$ within the plasma volume. The sign of $B_{\theta p}$ is inverted when the $j_z = 0$ condition is placed at a section downstream, e.g. in the presence of a dielectric target for material processing with MNs (cf. Fig. 8 of Ref. [6]). Notwithstanding this, observe that the magnetic force $\tilde{j}B_{\theta p}$ always acts in the outward direction in the plasma periphery, and therefore tends to increase plume divergence.

Figure 6 displays j_z and $B_{\theta p}$ for the simulation with $\beta_{a0} = 0.01$. A first observation is that while j_z becomes comparable to the ion current downstream, its absolute value is nonetheless small, and $B_{\theta p}$ is negligible in all cases of interest. Therefore, the azimuthal induced field is only a secondary feature of the near region expansion, compared to the longitudinal $\tilde{B}_p$. While the breakdown of isorotation described before (Eq. (4)) means a small change in $u_{\theta e}$ and the Hall force density on the electrons, $j_{\theta e}\tilde{B}\mathbf{1}_\perp$, the electron balance of forces is essentially unaffected by the presence of $B_{\theta p}$. Nonetheless, it couples the calculation of $u_{\theta e}$ with $u_{\parallel e}$, and it can lead to a large value of $u_{\theta e}$ especially in the neighborhood of a $B = 0$ point, if present.

To close this Section, it is noted that our plasma/MN model presents the following limitations related to the calculation of the induced field effects. First, the fully-magnetized electron model breaks down when the magnetic strength approaches zero. As the magnetic field diminishes, additional phenomena (resistivity, electron inertia, gyroviscous force[34, 30]) gain relevance in the electron equation of motion, which are neglected in the present model. These effects can initiate electron separation from the magnetic tubes and change their currents[14]. Consequently, the present model cannot provide a faithful description of the azimuthal currents when $B \to 0$, where a partially-magnetized electron model is needed.

Second, and associated to the previous point, the calculation of electron properties in the model is based on the propagation of the $H_e(\psi)$ function along magnetic lines ($\psi = \text{const}$). This function is defined at the MN throat from $\psi = 0$ (the axis) to $\psi = \psi_V$, the value at the plasma-vacuum edge. However, after the separatrix $\psi < 0$, and H_e is undefined. In the absence of a better criterion, here we have opted to maintain $H_e(\psi < 0) = H_e(0)$, under the assumption that the electrons that fill the region beyond the separatrix have a similar value of this integration constant than electrons at the axis. This, in particular, leads to $j_{\theta e} = 0$ in this region. The error committed by this is expected to be small within the simulated domain. Again, a partially-magnetized electron model is necessary to clarify the behavior of the plasma near and after the separatrix. Such model will also enable the closure of the longitudinal electric currents downstream.

Lastly, our gross Maxwellian, isotropic, isothermal electron model neglects the evolution of the electron velocity distribution function in the nozzle, which is affected by the set up of potential barriers[27]. While these aspects are important to obtain an accurate electron response, they are not expected to interfere with the central conclusions of the present work, which merely rely on the diamagnetic nature of the plasma expanding in the divergent field.

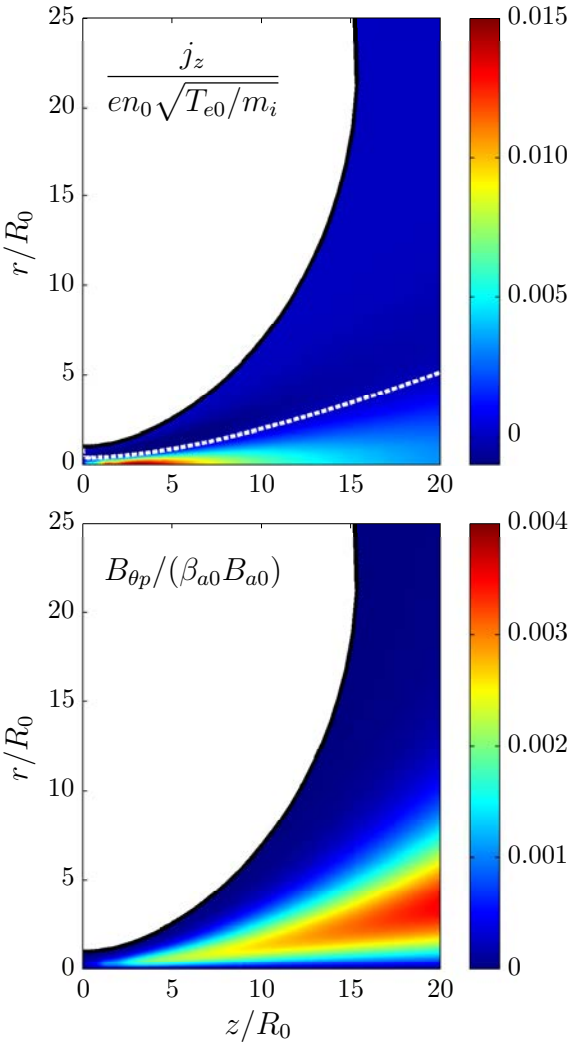

Figure 6. Axial electric current j_z and azimuthal induced magnetic field $B_{\theta p}/B$, in the $\beta_{a0} = 0.01$ case. The white dashed line in the first plot indicates the location where $j_z = 0$.

5. Conclusion

The two-fluid model of the plasma expansion in a divergent magnetic nozzle of Ref. [6] has been extended to include the plasma-induced magnetic field and study its effect on the expansion and the MN shape. An analytical analysis in the paraxial limit has been undertaken, followed by the full 2D numerical integration of the model to confirm and extend the conclusions of the 1D approximation. The induced field effects have been characterized as a function of β_{a0}, the main parameter in the discussion. The effect on $\boldsymbol{B}_p$ of an effective electron cooling rate, γ, has also been commented on. While the focus of the article are propulsive MNs in space plasma thrusters, its conclusions are easily

extrapolable to similar devices and configurations in plasma manufacturing, material processing and supersonic plasma wind tunnels.

It has been shown that the diamagnetic plasma-induced magnetic field, while essential for magnetic thrust generation, increases the aperture of the nozzle, resulting in a more divergent jet. At the same time, the induced field weakens the magnetic strength in the central part of the MN, and enhances the demagnetization of the core beam. Only in the case of an initially-hypersonic plasma or a very high level of ion magnetization (measured by $\hat{\Omega}_{i0}$ in the model) can the plasma become paramagnetic downstream, reinforcing the applied magnetic field while creating negative thrust (i.e. magnetic drag). The higher divergence deteriorates slightly the propulsive performance of the MN as measured by $\eta_{plume}(z)$.

A faster electron cooling rate (i.e., higher γ) reduces the magnitude of these effects. The induced magnetic field is markedly 2D, and concentrates in the region around the MN axis, while in the periphery of the plasma the magnetic field strength remains essentially constant. Already at rather small values of β_{a0}, the longitudinal induced field can cancel out the magnetic field at the axis of the jet, as observed experimentally[33], reversing its direction and forming a separatrix surface that marks the transition to an induced-field dominated region. The azimuthal induced field, on the other hand, is essentially negligible in most applications, but modifies the azimuthal electron current where the longitudinal field is low. This effect decreases with increasing $\hat{\Omega}_{i0}$.

Acknowledgments

The authors would like to thank Manuel Martínez-Sánchez for the insightful discussions. Initial work was sponsored by the Air Force Office of Scientific Research, Air Force Material Command, USAF (FA8655-12-1-2043). Additional support was provided by Spanish R&D National Plan (grant number ESP2013-41052-P). Preliminary versions of this work were presented in a conference[32].

References

[1] Andersen S, Jensen V, Nielsen P and D'Angelo N 1969 *Phys. Fluids* **12** 557–560
[2] Kuriki K and Okada O 1970 *Physics of Fluids* **13** 2262
[3] York T M, Jacoby B A and Mikellides P 1992 *Journal of Propulsion and Power* **8** 1023–1030
[4] Inutake M, Ando A, Hattori K, Tobari H and Yagai T 2002 *J. Plasma Fusion Res.* **78** 1352–1360
[5] Takama Y and Suzuki K 2008 *Plasma Sources Science and Technology* **17** 015005
[6] Ahedo E and Merino M 2010 *Physics of Plasmas* **17** 073501 ISSN 1089-7674
[7] Krülle G, Auweter-Kurtz M and Sasoh A 1998 *J. Propulsion and Power* **14** 754–763
[8] Arefiev A and Breizman B 2004 *Physics of Plasmas* **11** 2942–2949
[9] Charles C and Boswell R 2003 *Applied Physics Letters* **82** 1356
[10] Prager J, Winglee R, Ziemba T, Roberson B and Quetin G 2008 *Plasma Sources Science and Technology* **17** 025003
[11] Batishchev O 2009 *IEEE Transaction on Plasma Science* **37** 1563–1571
[12] Ahedo E 2011 *Plasma Physics and Controlled Fusion* **53** 124037 URL `http://stacks.iop.org/0741-3335/53/i=12/a=124037`

[13] Gerwin R, Marklin G, Sgro A and Glasser A 1990 Characterization of plasma flow through magnetic nozzles Tech. Rep. AFSOR AL-TR-89-092 Los Alamos National Laboratory
[14] Ahedo E and Merino M 2011 *Physics of Plasmas* **18** 053504 ISSN 1089-7674
[15] Merino M and Ahedo E 2014 *Plasma Sources Science and Technology* **23** 032001 ISSN 0963-0252
[16] Hoyt R, Scheuer J, Schoenberg K, Gerwin R, Moses R and Henins I 1995 *IEEE Transactions On Plasma Science* **23** 481–494
[17] Schoenberg K, Gerwin R, Moses R, Scheuer J and Wagner H 1998 *Physics of Plasmas* **5** 2090–2104
[18] Longmier B, Bering E, Carter M, Cassady L, Chancery W, Díaz F, Glover T, Hershkowitz N, Ilin A, McCaskill G *et al.* 2011 *Plasma Sources Science and Technology* **20** 015007
[19] Arefiev A and Breizman B 2005 *Physics of Plasmas* **12** 043504
[20] Winglee R, Ziemba T, Giersch L, Prager J, Carscadden J and Roberson B 2007 *Physics of Plasmas* **14** 063501
[21] Merino M, Ahedo E, Bombardelli C, Urrutxua H and Peláez J 2011 Hypersonic plasma plume expansion in space *32nd International Electric Propulsion Conference* IEPC-2011-086 (Fairview Park, OH: Electric Rocket Propulsion Society)
[22] Takahashi K, Lafleur T, Charles C, Alexander P and Boswell R 2011 *Physical Review Letters* **107** 235001
[23] Merino M and Ahedo E 2013 *Physics of Plasmas* **20** 023502 ISSN 1089-7674
[24] Merino M and Ahedo E 2015 *IEEE Transactions on Plasma Science* **43** 244–251 ISSN 0093-3813
[25] Deline C, Bengtson R, Breizman B, Tushentsov M, Jones J, Chavers D, Dobson C and Schuettpelz B 2009 *Physics of Plasmas* **16** 033502
[26] Sheehan J P, Longmier B W, Bering E A, Olsen C S, Squire J P, Ballenger M G, Carter M D, Cassady L D, Díaz F R C, Glover T W and Ilin A V 2014 *Plasma Sources Science and Technology* **23** 045014 URL `http://stacks.iop.org/0963-0252/23/i=4/a=045014`
[27] Martinez-Sanchez M, Navarro-Cavallé J and Ahedo E 2015 *Physics of Plasmas* **22** 053501
[28] Hu Y and Wang J 2015 *Plasma Science, IEEE Transactions on* **43** 2832–2838 ISSN 0093-3813
[29] Chandrasekhar S 1956 *The Astrophysical Journal* **124** 232
[30] Ahedo E and Merino M 2012 *Physics of Plasmas* **19** 083501 ISSN 1089-7674
[31] Merino M and Ahedo E 2016 *Physics of Plasmas* **23** 023506 ISSN 1089-7674
[32] Merino M and Ahedo E 2011 Plasma detachment mechanisms in a magnetic nozzle 47^{th} *AIAA/ASME/SAE/ASEE Joint Propulsion Conference & Exhibit* AIAA-2011-5999 (Washington DC: AIAA) ISBN 978-1-60086-949-5
[33] Roberson B, Winglee R and Prager J 2011 *Physics of Plasmas* **18** 053505
[34] Ramos J 2005 *Physics of plasmas* **12** 112301